Computer Modeling in Engineering & Sciences

Tech Science Press

https://doi.org/10.32604/cmes.2026.088142

ARTICLE

A New EEG Emotion Detection Model Based on Multichannel Binary Transition Pattern

Abdullahi Abba Abdullahi[1], Suat Tas[1], Dahiru Tanko[1], Gullu Boztas[2], Burak Tasci[3,*], İrem Taşcı[4], Sengul Dogan[1] and Turker Tuncer[1]

[1]Department of Digital Forensics Engineering, College of Technology, Firat University, Elazig, Turkey
[2]Department of Electrical and Electronics Engineering, Faculty of Technology, Firat University, Elazig, Turkey
[3]Vocational School of Technical Sciences, Firat University, Elazig, Turkey
[4]Department of Neurology, School of Medicine, Firat University, Elazig, Turkey

*Corresponding Author: Burak Tasci. Email: btasci@firat.edu.tr

Received: 01 July 2026; Accepted: 09 September 2026; Published: 21 October 2026

ABSTRACT: Electroencephalography (EEG) emotion recognition attempts to infer affective state from brain activity. This work proposes multichannel Binary Transition Pattern (mBTP), a BP-derived descriptor that converts center-to-neighbor vector differences into ordered channel transitions and transition-table features. We also introduce a text-elicited EEG emotion dataset collected from 49 participants, with 245 records divided into 4895 15-s segments representing five emotions. The resulting explainable feature-engineering pipeline combines mBTP with cumulative weighted neighborhood component analysis (CWNCA), t-algorithm-based k-nearest neighbors (tkNN), and Directed Lobish (DLob). On the five-class task, the complete pipeline reached 88.50% accuracy under segment-level 10-fold cross-validation and 75.12% under leave-one-record-out (LORO) validation. Controlled ablations yielded 82.29% with BP, 84.11% with LBP, 86.09% after replacing CWNCA with NCA, and 86.82% after replacing tkNN with a single kNN. These results describe internal segment- and record-level validation and should not be read as subject-independent LOSO performance. Overall, mBTP provides a compact and interpretable EEG representation, while repeated-seed testing, participant-disjoint LOSO, and matched public-benchmark evaluation remain important next steps.

KEYWORDS: Multichannel binary transition pattern; explainable feature engineering; EEG emotion recognition; directed lobish; EEG signal classification; connectome theory

1 Introduction

Electroencephalography (EEG) provides a non-invasive measurement of brain activity and is widely used because of its portability and high temporal resolution [1,2]. EEG signals can also support the monitoring and analysis of brain activity and related abnormalities. Even so, reliable interpretation remains challenging because these signals are complex and vary over time and across individuals [3].

Signal noise, between-person variability, and time-varying EEG dynamics further complicate analysis [4]. Effective preprocessing and feature extraction are therefore important for reducing noise and identifying salient EEG features for accurate classification [5]. Recent signal-processing and machine-learning studies have increasingly focused on feature representations and classifiers that remain effective under these conditions [6,7].

Copyright © 2026 The Authors. Published by Tech Science Press. This work is licensed under a Creative Commons Attribution 4.0 International License, which permits unrestricted use, distribution, and reproduction in any medium, provided the original work is properly cited.

Feature engineering offers a practical alternative to fully deep models when interpretability and computational cost are important [8–10]. Well-designed descriptors can capture spatial and temporal information without requiring a large end-to-end network [11]. Well-designed descriptors can capture spatial and temporal information without requiring a large end-to-end network. This balance is especially relevant for systems intended for timely or resource-constrained clinical use [12].

Against this background, this work examines a compact pipeline that couples a new multichannel feature descriptor with feature selection, classification, and symbolic interpretation. The aim is not only to classify EEG emotion patterns accurately, but also to make the selected channel relationships easier to inspect.

1.1 Related Work and Current Challenges

Recent EEG emotion-recognition research encompasses both computationally intensive deep-learning approaches and more explicit feature-engineering strategies. This section reviews these complementary directions in two parts: Section 1.1.1 summarizes recent deep, graph-based, and domain-adaptation methods, whereas Section 1.1.2 discusses lightweight feature-engineering approaches and the role of interpretability. Together, these perspectives establish the methodological context for the research gaps addressed in this study.

1.1.1 Deep, Graph-Based, and Domain-Adaptation Approaches

Recent EEG emotion-recognition studies cover graph learning, domain adaptation, spectral representations, and deep ensembles. Fu et al. [13] modeled SEED differential-entropy features with dynamic graph attention and reported 91.65% subject-dependent and 85.86% cross-subject accuracy; the evaluation was limited to one benchmark. Bagherzadeh et al. [14] fused effective-connectivity maps in an ensemble deep model, reaching 98.76% on Database for Emotion Analysis using Physiological Signals (DEAP) and 98.86% on MAHNOB-HCI, although the small cohorts and model-tuning cost may restrict generalization. Cai et al. [15] transformed EEG into spectral images for SEED and SEED-IV. Their subject-dependent accuracies were 94.83% and 79.45%, while the corresponding subject-independent results were 80.07% and 66.72%; imbalanced-data behavior was not examined. Han et al. [16] used a multi-scale deep architecture on DEAP and obtained 91.31% for arousal and 90.45% for valence in subject-dependent tests, with 86.66% and 85.40% in subject-independent evaluation; validation across additional datasets was not reported. Bardak et al. [17] combined predefined EEG features with a hybrid classifier and reported 95.97% on the feeling-emotions dataset and 73.49% on DEAP. Yu et al. [18] addressed cross-subject and cross-session recognition on SEED and SEED-IV with multi-source domain adaptation, obtaining 90.96% and 91.94% for cross-subject tests and 76.01% and 78.78% for cross-session tests, at the cost of a more complex pipeline. Shi and Liu [19] evaluated an interactive multi-agent convolutional broad-learning system on DEAP, DREAMER, and SEED, with accuracies of 82.86%, 98.49%, and 85.09%. Dai et al. [20] reported 95.23% valence and 96.31% arousal accuracy on DEAP and 95.16% on SEED using a contrastive EEG representation. Xiao et al. [21] tested dynamic contrastive domain adaptation on SEED and SEED-IV, reporting 90.84% and 78.49% in cross-subject experiments and 95.82% and 82.25% across sessions; the method adds substantial computational complexity. Cruz-Vazquez et al. [22] collected EEG from 40 participants and reported 95.00% accuracy, but did not provide validation on a public benchmark. Zhang et al. [23] used four-dimensional feature representations and attention, reaching 92.41% valence and 92.71% arousal accuracy on DEAP and 93.93% on SEED; the approach depends on predefined feature mappings. Sun et al. [24] reported 83.50% subject-independent and 88.93% subject-dependent accuracy on HR-EEG4EMO, using a high-density EEG setting. Wang et al. [25] obtained 98.51% on DEAP, 98.01% on DREAMER, and 97.30% on SEED with a transformer-based model, although this performance comes with a relatively heavy computational design. Tan et al. [26]

addressed cross-subject analysis on SEED and SEED-IV and achieved 86.39% and 77.80%, respectively; their workflow relies on offline feature decomposition. Gao et al. [27] used low-rank self-representation features on DEAP and reported 93.04% for valence, 93.13% for arousal, and 88.82% for four-class recognition; preservation of spatial channel information remained limited. Chen et al. [28] combined differential entropy and power spectral density with a 3D feature-fusion network. Under 10-fold CV, they reported 84.93% arousal and 83.54% valence accuracy on DEAP and 96.64% on SEED, with evaluation restricted to a small set of datasets. Chaudary et al. [29] presented an interpretable deep model on SEED and reported 99.31% accuracy, but did not test additional datasets. Hu et al. [30] used contrastive learning for cross-subject recognition on SEED, THU-EP, and FACED, reporting 88.3% for three-class SEED, 76.2% for nine-class THU-EP, and 72.5% for binary FACED; the method uses high-dimensional EEG features. Ju et al. [31] applied domain-adversarial learning to SEED and SEED-IV and reached 95.74% and 86.75%, while relying on a limited set of calibration samples. Cao et al. [32] combined multi-scale EEG features with graph convolutional attention and reported 95.2% on SEED and 86.2% on TJU-EmoEEG; the approach was evaluated with high-density EEG. Xu et al. [33] modeled differences in cortical temporal scales across DEAP, DREAMER, and PhyMER, obtaining 77.11%/76.71%, 82.78%/80.79%, and 86.41%/82.13% for valence/arousal, respectively; the pipeline requires extensive feature engineering. Li et al. [34] reported 97.55% valence and 97.61% arousal accuracy on DEAP, with no second dataset used for external comparison. Chang et al. [35] evaluated hyperbolic contrastive learning on SEED, MPED, and FACED, obtaining 89.3% for three-class SEED, 38.8% for seven-class MPED, and 77.0%/45.7% for binary/nine-class FACED; the representation is high dimensional. Chen et al. [36] combined 3DCNN-CapsNet with hierarchical attention and reported 97.40% valence, 97.20% arousal, and 97.60% dominance accuracy on DEAP, plus 95.80%, 96.10%, and 96.30% on DREAMER; predefined frequency-band weighting remains part of the design. Yan et al. [37] used a spatio-temporal graph BERT model and obtained 89.39% on SEED and 80.32% for DEAP arousal classification, with performance tied to a predefined subgraph partition. Hu et al. [38] described a multi-perspective spatio-temporal EEG framework for audio-visual perceptual quality assessment that combines temporal, regional, and global representations with diffusion-based augmentation. Jiang et al. [39] developed a fuzzy federated ensemble for EEG emotion recognition in the Internet of Medical Things, integrating Temporal Convolutional Network (TCN), Long Short-Term Memory (LSTM), and Gated Recurrent Unit (GRU) components while retaining a privacy-preserving distributed setting. Taken together, the literature shows strong progress, but reported accuracies come from different datasets, class definitions, channel layouts, and validation schemes. Computational burden, reliance on high-dimensional representations, limited interpretability, and cross-subject generalization therefore remain recurring issues. Text-based emotion elicitation is also less common than audiovisual stimulation, leaving room for compact and interpretable methods designed for this setting.

1.1.2 Lightweight Feature-Engineering and Explainability Perspective

Two broad trends are apparent in the reviewed work. One uses deep, graph-based, attention, or domain-adaptation models; the other relies on explicit spectral or handcrafted representations. Both can perform well, but their reported numbers cannot be compared directly because the datasets, label definitions, and validation units differ. Our work follows the explicit-representation route and focuses on preserving channel-transition structure while keeping the final explanation at the sensor-symbol level. Table 1 provides a concise view of representative studies and their validation settings.

Table 1: Representative recent EEG emotion-recognition studies and their validation settings.

Study	Dataset	Method Family	Validation	Reported Accuracy (%)	Main Limitation Relevant Here
Fu et al. [13]	SEED	Dynamic graph attention	Cross-subject/ LOSO-type	85.86 cross-subject	Single benchmark dataset
Bagherzadeh et al. [14]	DEAP; MAHNOB-HCI	Ensemble deep learning + effective connectivity	Reported LOSO	98.76; 98.86	Higher model complexity; small cohorts
Cai et al. [15]	SEED; SEED-IV	EEG spectral image + transformer	Subject-dependent/independent	94.83/80.07; 79.45/66.72	Performance varies across datasets/settings
Yu et al. [18]	SEED; SEED-IV	Multi-source domain adaptation	Cross-subject/cross-session	90.96/91.94; 76.01/78.78	Increased computational complexity
Gao et al. [27]	DEAP	Feature-based EEG emotion recognition	Binary and four-class	93.04 valence; 93.13 arousal; 88.82 four-class	Limited preservation of spatial channel information
Chaudary et al. [29]	SEED	Deep model with XAI	Single dataset	99.31	External generalization not established

1.2 Research Gaps

- EEG emotion datasets are now numerous [35,40,41], but only a smaller group is used repeatedly as common benchmarks. Many of these datasets elicit emotion with video or other audiovisual material [40,42]. Here, we instead examine whether short written sentences can provide a useful five-class elicitation setting.
- High-performing EEG emotion-recognition studies often rely on deep architectures [43,44]. These models can be effective, yet their computational cost can be substantial [44], which motivates a lighter feature-engineering alternative.
- Explainability remains less common than accuracy-focused model development in EEG emotion recognition [45,46]. For this reason, the present pipeline includes an explicit symbolic interpretation stage rather than treating explanation as a separate *post-hoc* add-on.

We therefore introduce multichannel Binary Transition Pattern (mBTP), a multichannel EEG descriptor derived from BP. The prefix “m” is retained throughout the paper to distinguish this method from the earlier Binary Transition Pattern (BTP) terminology used for temporal DNA methylation coding. That earlier BTP encodes stage-wise methylation changes with fixed binary sequences, whereas mBTP operates on multichannel physiological signals. Specifically, mBTP forms overlapping EEG blocks, computes center-to-neighbor vector differences, orders channel identities, and converts the resulting transitions into transition-table features.

The first gap is addressed through a sentence-elicited EER dataset containing 4895 EEG segments in five classes. This collection provides a balanced text-based setting that complements the audiovisual protocols used by many established datasets.

The second gap is addressed with an explicit feature-engineering pipeline built to test mBTP on the collected EEG emotion data rather than relying on an end-to-end deep architecture.

For the third gap, Directed Lobish (DLob) [47] is incorporated as the interpretation layer. This gives the model an explainable feature-engineering (XFE) output in addition to its classification result.

The XFE pipeline has four stages. First, mBTP extracts the multichannel transition features. CWNCA then selects the most informative subset. The selected features are passed to tkNN for classification and, in parallel, their identities are mapped to DLob for symbolic interpretation. Classification is evaluated with segment-level 10-fold cross-validation (CV) and leave-one-record-out (LORO) CV. The DLob branch converts the selected feature identities into a symbolic sequence from which the channel-level connectome representation is derived.

1.3 Major Contributions and Paper Organization

Innovations:

- A five-class EER dataset was collected using sentence-based emotion elicitation.
- BP was extended from scalar comparisons to a multichannel form, termed mBTP.
- mBTP was combined with CWNCA, tkNN, and DLob in one XFE pipeline so that classification and channel-level interpretation could be examined together.

Contributions:

- The resulting mBTP-based XFE model provides a compact feature representation and strong internal performance under both 10-fold CV and LORO CV.
- DLob adds a second view of the selected features by expressing their channel-level transition structure in symbolic form. This supports interpretation of the model output without treating the resulting diagrams as direct neurophysiological connectivity measurements.

The rest of the paper is arranged as follows. Section 2 describes the EEG dataset and acquisition setting. Section 3 defines mBTP, and Section 4 explains the complete feature-engineering pipeline. Section 5 reports the experiments, Section 6 discusses the findings and comparisons, and Section 7 summarizes the study.

2 Material

A text-based EEG emotion dataset was collected from 49 Turkish participants with an Emotiv EPOC 14-channel headset. The recording session produced 245 records, later divided into 4895 segments of 15 s. Participants sat comfortably and silently repeated each sentence displayed on the screen. A 1-min rest interval separated consecutive recordings to reduce carry-over from the preceding stimulus. The protocol was approved by the Non-Invasive Ethics Committee of Firat University on 04 November 2021 (approval no. 2021/11-34), followed the Declaration of Helsinki, and included written informed consent from every participant.

The sentences in Table 2 were used as the emotion-elicitation stimuli. After acquisition, each EEG record was divided into 15-s segments. Table 3 summarizes the main properties of the resulting dataset.

Table 2: English translations of the sentences used to elicit emotions.

Emotion	Number	Sentence	Original Turkish Sentence
Neutral	1	Hello, welcome!	Merhaba, hoş geldiniz!
	2	Take it easy.	Rahat ol.
	3	Take care!	Kendine iyi bak!
	4	See you soon!	Yakında görüşürüz!
	5	Good evening!	İyi akşamlar!

(Continued)

Table 2 (continued)

Emotion	Number	Sentence	Original Turkish Sentence
Happy	1	I'm so happy!	Çok mutluyum!
	2	How lucky I am!	Ne kadar şanslıyım!
	3	That's fantastic news.	Bu harika bir haber.
	4	I'm feeling so excited!	Çok heyecanlı hissediyorum!
	5	Everything is perfect!	Her şey mükemmel!
Sad/Negative	1	I feel overwhelmed.	Bunalmış hissediyorum.
	2	My soul feels suffocated.	Ruhum daralıyor.
	3	I'm feeling down.	Kendimi kötü hissediyorum.
	4	I'm truly sad.	Gerçekten üzgünüm.
	5	I feel lost.	Kendimi kaybolmuş hissediyorum.
Angry	1	I'm losing my patience!	Sabrımı kaybediyorum!
	2	I'm furious!	Çok öfkeliyim!
	3	My patience is running out.	Sabrım tükeniyor.
	4	That's enough already!	Artık yeter!
	5	Get out of my way!	Yolumdan çekil!
Surprise	1	I'm shocked!	Şok oldum!
	2	I can't believe my eyes!	Gözlerime inanamıyorum!
	3	I can't wrap my head around this!	Bunu aklım almıyor!
	4	This can't be real!	Bu gerçek olamaz!
	5	No way!	Olamaz!

Table 3: The characteristics of the collected dataset.

Features	Value
Gender	37 Males, 12 Females, Total: 49
Age	Minimum: 19, Maximum: 26, Overall: 23.15 ± 1.20
Nationality	Turkish
Distribution (Number of EEG segments)	1- Neutral: 978 2- Happy: 980 3- Sad: 978 4- Angry: 980 5- Surprise: 979 Total: 4895

Fig. 1 confirms that the five classes are almost evenly represented at the segment level. The plot is limited to class counts and should not be interpreted as a spectral or amplitude-distribution analysis of the raw EEG.

This dataset is a distinct contribution of the study because it uses five sentence-elicited emotion classes rather than the audiovisual stimulation adopted in many widely used EEG emotion resources.

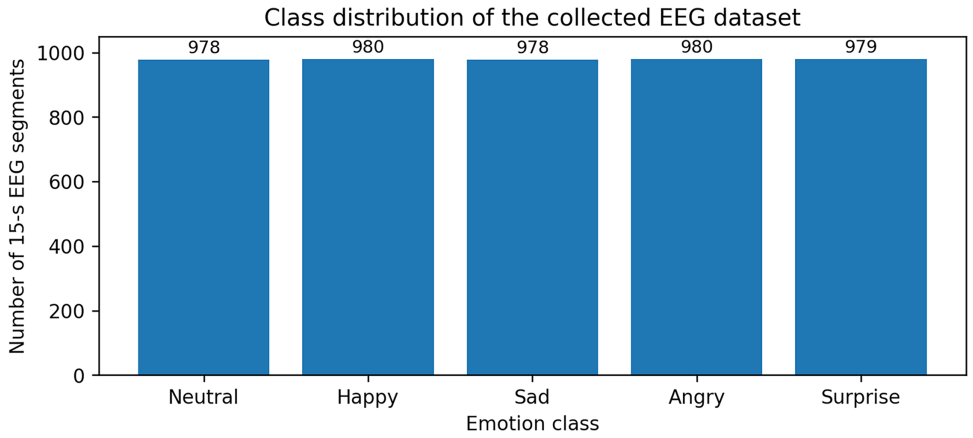


Figure 1: Distribution of the 4895 15-s EEG segments across the five emotion classes. The class counts are nearly balanced: neutral = 978, happy = 980, sad = 978, angry = 980, and surprise = 979.

3 Multichannel Binary Transition Pattern

This work introduces multichannel Binary Transition Pattern (mBTP), a BP-derived descriptor for multichannel EEG. The name separates the proposed signal-processing method from the earlier Binary Transition Pattern (BTP) terminology used in DNA methylation analysis. Whereas the earlier BTP encodes changes between methylation stages, mBTP builds transition-table features from ordered channel identities. For the 14-channel montage used here, each overlapping input block has a size of 9×14.

mBTP replaces the scalar neighborhood used by BP with nine channel vectors. The fifth vector is the center. Each of the other eight vectors is subtracted from this center, producing eight difference vectors of size 1×14 (or $1 \times$ n for an n-channel input).

Each difference vector is converted to an ordered channel sequence. A transition table is then formed for that sequence, yielding eight tables in total. Flattening the tables and concatenating their entries produces the final mBTP feature vector.

Fig. 2 gives an overview of the mBTP feature-extraction process.

The same procedure is described step by step below.

S1: Initialize the transition table used by mBTP.

$$tt_b = \begin{bmatrix} 0 & \cdots & 0 \\ \vdots & \ddots & \vdots \\ 0 & \cdots & 0 \end{bmatrix}, b \in \{1, 2, \ldots, 8\} \tag{1}$$

herein, tt: transition table with a size of $n \times n$ and n: the number of channels.

S2: Create overlapping matrices.

$$m^h = signal\,(h{:}\,h+8, 1{:}\,n)\,, h \in \{1, 2, \ldots, \ell - 8\} \tag{2}$$

herein, m: the created overlapped matrix with a size of $9 \times n$, $signal$: the used signal for feature extraction and ℓ: length of the signal utilized.

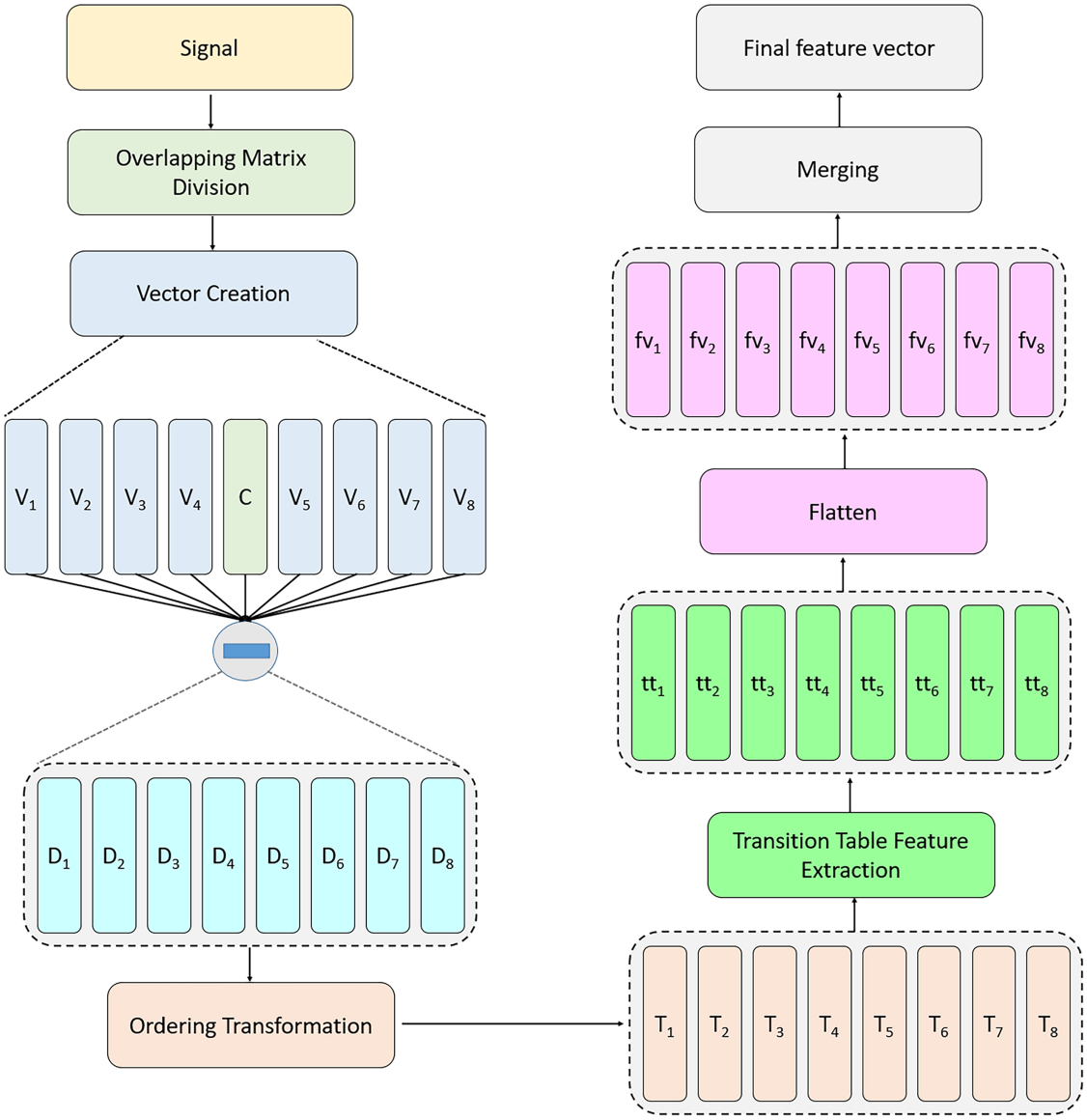


Figure 2: The graphical overview of the introduced mBTP feature extraction function. Herein, V: vector, D: difference vector, T: transformed vector, tt: transition table, fv: individual feature vector.

S3: Create vectors deploying the overlapped matrix created.

$$v_k^h = m^h(k,:), k \in \{1,2,3,4\} \tag{3}$$

$$center^h = m^h(5,:) \tag{4}$$

$$v_{k+4}^h = m^h(k+5,:) \tag{5}$$

where v: the vectors computed and $center$: the center (5th) vector.

S4: Compute the differences vectors.

$$dif_b^h = v_b^h - center^h \tag{6}$$

Here, $diff$: the difference vector. The subtraction follows the BP center-neighbor idea, but operates on channel vectors rather than scalar values. BP converts scalar differences with a sign function, whereas mBTP orders channel identities and counts their transitions. The next steps describe this conversion.

S5: Apply ordering/channel transformer to obtain transformed signals.

$$T_b\left(x{:}\,x+n-1\right)=argsort\left(-dif_b^h\right),x\in\{1,n+1,\ldots,n\left(h-1\right)+1\} \tag{7}$$

where T: transformed signal. Applying the ordering operation to the eight difference vectors yields eight transformed channel-identity sequences.

S6: Repeat S2–S5 for all eight neighbor positions.

S7: Build one transition-table feature vector from each transformed signal.

$$tt_b\left(T_b(i),T_b\left(i+1\right)\right)+=1,i\in\{1,2,\ldots,\mathcal{L}-1\} \tag{8}$$

herein, tt: transition table generated and $\mathcal{L}$: length of the transformed signal.

S8: Flatten the eight transition tables into individual feature vectors.

$$fv_b(y)=tt_b\left(q,w\right),q\in\{1,2,\ldots,n\},w\in\{1,2,\ldots,n\},y\in\left\{1,2,\ldots,n^2\right\} \tag{9}$$

herein, fv: the generated individual feature vector with a length of n^2.

S9: Concatenate the eight individual feature vectors.

$$feat\left(y+n^2\times\left(b-1\right)\right)=fv_b(y) \tag{10}$$

where $feat$: the created final feature vector with a length of $8n^2$.

These nine steps define mBTP. Each feature counts how often one channel identity follows another within one of the eight transformed sequences. For example, one feature can count channel 1-to-channel 2 transitions in the first sequence, while another can count channel 5-to-channel 9 transitions in the fourth. Because every transformed sequence yields a 14 × 14 table, each route contributes 196 features and the eight routes together produce 1568 features per EEG segment.

4 mBTP-Centric Explainable Feature Engineering

To test mBTP within a complete classifier, we place it inside an explainable feature-engineering (XFE) pipeline with four stages:

- mBTP-based feature extraction
- CWNCA-based feature selection
- tkNN-based classification
- DLob-based XAI results generation

Fig. 3 shows the full mBTP-centric XFE pipeline.

The four stages are described next.

Phase 1: Feature extraction: mBTP is applied to every EEG segment, producing 1568 (=14 × 14 × 8) features per segment. Section 3 gives the construction in detail. The resulting vectors form the feature matrix used by the next stage. All preprocessing, CWNCA feature selection, feature-count determination, kNN parameter ranking, and IMV construction were performed using only the training data within each cross-validation fold.

$$X(p,:) = mBTP\left(signal_p\right), p \in \{1, 2, \ldots, Dim\} \tag{11}$$

where X: the feature matrix created, $BTP(.)$: the mBTP feature extraction function and Dim: the number of EEG signals.

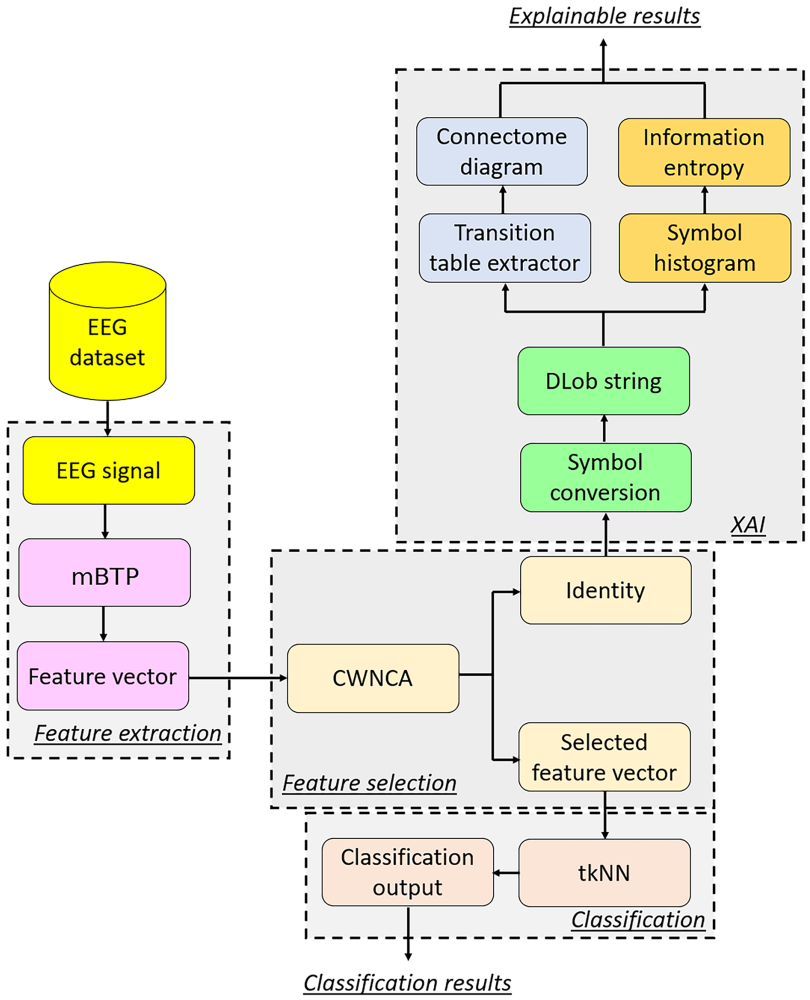


Figure 3: The introduced mBTP-centric XFE framework's graphical depiction.

Phase 2: Feature selection: CWNCA selects a compact subset of informative features. CWNCA extends neighborhood component analysis (NCA) [48] by using cumulative feature weights to determine the retained dimension. In this experiment, the cumulative-weight threshold is 0.9. The procedure returns both the selected feature matrix and the original feature identities, which are later used by DLob. Algorithm 1 summarizes the selection process.

$$[ind, SelX] = CWNCA(X, out, 0.9) \tag{12}$$

where, idx the the indices of the selected features, $SelX$: the chosen feature matrix, $CWNCA(.)$: the CWNCA feature selection function and out: the class labels. A cumulative-weight threshold of 0.9 was used to determine the retained feature count. Algorithm 1 summarizes the CWNCA selection procedure.

Algorithm 1: The CWNCA feature selection function

Input: The generated feature matrix, threshold value and the actual outcome.
Output: The final selected feature matrix and identities of this selected feature matrix.

01: $X = \frac{X-\min(X)}{\max(X)-\min(X)+\varepsilon}$ // Applying min-max normalization.
02: $[wg, idx] = NCA(X, out)$ // Create the weights (wg) and qualified identities (idx).
03: $opt = CW(X, out, wg, 0.9)$ // Compute the optimal number of the features.
// where opt: the optimal number of the features, $CW(.)$: cumulative weight computation function
04: $SelX = X(:, idx(1{:}opt))$ // Creating selected feature matrix.
05: $ide = idx(1{:}opt)$
// Creating the identities of the selected features. Here, ide denotes the identities of the selected features.

Algorithm 1 retained 281 of the 1568 mBTP features.

Phase 3: Classification: tkNN provides the classification stage; standard kNN [49] is used only as its base learner and is not claimed as a new contribution. tkNN evaluates multiple combinations of distance metric, distance weighting, and neighborhood size, ranks their cross-validation results, and then creates additional ensemble outcomes with iterative majority voting (IMV) [50]. The final output is the individual or voted prediction with the highest observed classification accuracy. Algorithm 2 documents this procedure.

$$outcome = tkNN(SelX, out, Params) \tag{13}$$

herein, $outcome$: the created classification outcome, $tkNN(.)$: the tkNN classifier employed and $Params$: the parameter set. Algorithm 2 gives the tkNN pseudocode.

Algorithm 2: Implementation procedure of the tkNN classifier used in the proposed framework

Input: The chosen feature matrix and actual outcome.
Output: The final classification outcome.

01: $Dst = \{Cityblock, Cosine, Euclidean\}$; // The used distance table.
02: $W = \{SquaredInverse, Inverse, Equal\}$ // The utilized weights (W) table.
03: $c = 1$; // Counter definition
04: **for** k = 1 to 10 **do** // k values
05: **for** i = 1 to 3 **do** // To choose distance parameters
06: for j = 1 to 3 do // To choose weight parameters
07: $pt_c = kNN(SelX, out, k, Dst(i), W(j))$
// Parameter-based outcomes (pt) generation.
08: $acc(c) = A(pt_c, out)$ // Herein, $A(.)$: the accuracy computation function.
09: $c+ = 1$; // Increasing counter.
10: **end for j**
11: **end for i**
12: **end for k**
13: $q = argsort(-acc)$ // where, q: the sorted indexes of the accuracies computed.
14: **for** j = 3 to c−1 **do** // IMV iteration.
15: $vt_{i-2} = mode(pt_{q(1)}, pt_{q(2)}, \ldots, pt_{q(i)})$
16: $acc(c + j - 3) = A(vt_{j-2}, y)$ // Classification accuracy computation.

(Continued)

Algorithm 2 (continued)

// Herein, $mode(.)$: the utilized mode function and vt: voted outcome computed.
17: **end for j**
18: $\alpha = argmax(acc)$ // Herein, β: the identity of the maximum classification accuracy.
19: **if** $\alpha < c$ **then**
20: $outcome = pt_{\alpha}$
21: **else**
22: $outcome = vt_{\alpha-c+1}$
23: **end if**

The implementation evaluates 90 kNN configurations: three distances (cityblock, Euclidean, and cosine), three weighting rules (squared inverse, inverse, and equal), and ten neighborhood sizes (k = 1, ..., 10). Thus, 3 × 3 × 10 = 90 parameterized models are ranked by 10-fold cross-validation accuracy before the IMV outcomes are formed.

The ranked tkNN procedure is then used to obtain the classification output.

Phase 4: XAI: DLob summarizes the selected channel relationships with a symbolic vocabulary. The general vocabulary contains 16 symbols: FL, FR, Fz, TL, TR, PL, PR, Pz, CL, CR, Cz, OL, OR, Oz, AL, and AR. For the 14-channel Emotiv EPOC montage used here, eight regional symbols are instantiated: FL, FR, TL, TR, PL, PR, OL, and OR. The other symbols remain part of the general DLob language but are not mapped in this dataset. In particular, AL and AR are not assigned to the EPOC reference electrodes. Selected mBTP feature identities are mapped to the applicable symbols through a lookup table, after which the DLob string is summarized by a histogram, transition table, Shannon entropy, and channel-level connectome view. These outputs describe selected sensor transitions and are not source-localized measurements of cortical activity.

Algorithm 3 summarizes the DLob-based interpretation stage used in this study.

Algorithm 3: The DLob-based XAI method

Input: The identities of the selected features (ide) and the LUT created according to the used brain cap (LUT)
Output: The DLob string (ds), histogram of the utilized symbols ($histogram$), connectome diagram ($cond$) and Information Entropy ($infent$).

01: cnt = 1; // Definition of the counter.
02: Define initial values of the histogram, transition table and Shannon Entropy value.
03: **for** i = 1 to λ **do** // Herein, λ: the length of the chosen feature vector.
04: $c_1 = \left\lfloor \frac{ide(i)-1}{n} \right\rfloor (modn) + 1$
05: $c_2 = ide(i) - 1\ (modn) + 1$
// c: the first and second channel values of the chosen features. By deploying digit separation, these values have been computed.
06: $ds\,(cnt) = LUT\,(c_1)$ // Channel to DLob symbol convertion.
07: $ds\,(ct+1) = LUT\,(c_2)$
08: $histogram\,(ds\,(ct))$ + = 1 // Increasing histogram value.
09: $histogram\,(ds\,(ct+1))$ + = 1
10: cnt+ = 2; // Increasing counter.
11: **end for i**

(Continued)

Algorithm 3 (continued)

// In this loop (lines 03–11), DLob string has been generated
12: **for** j = 1 to $2\lambda-1$ **do**
13: $trt\left(ds(j), ds\left(j+1\right)\right) += 1$;
// where trt: transition table of the DLob symbols. This transition table has been created to obtain cortical connectome diagram.
14: **end for j**
15: **for** j = 1 to n **do**
16: $prb(i) = \frac{histo(i)}{\sum_{k=1}^{n} histo(k)}$ // Herein, prb: probability.
17: $infent += pr(i) \times \log\left(pr(i)\right)$ // Computing information entropy
18: **end for j**
19: $infent = -infent$;
20: Visualize trt to depict cortical connectome diagram and create $cond$.

5 Experimental Results

This section reports the classification and interpretation results of the mBTP-centric XFE pipeline. The experiments were run in MATLAB 2024a on a Windows 11 computer with 16 GB RAM and a 2.8 GHz processor. The implementation uses separate m-files for the main stages. The main routine loads each EEG segment, calls mBTP to form the feature matrix, applies CWNCA to obtain the selected features and their identities, sends the selected values to tkNN, and passes the identities to the DLob interpretation routine.

The pipeline is parameter-based but remains computationally modest. Table 4 lists the main settings and the associated time-complexity terms.

Table 4: Parameters and time burden of the mBTP-centric XFE framework.

Phase	Method	Parameters	Time Burden
Feature extraction	mBTP	The size of the overlapped matrix: $9 \times n$, Distance computation technique: Subtraction of the center vector from neighbor vectors, Transformation method: Channel/Ordering transformer, Feature extraction function: Transition table-based feature extraction, The length of the generated feature: $8 \times n^2$	$O(E)$
Feature selection	CWNCA	Input: Generated feature vector, Threshold value: 0.9	$O\left(N+F\right)$
Classification	tkNN	Number of parameters: 90 (3 distances × 3 weights × 10 k values) Voting method: IMV, Number of voted outcomes: 88, The number of total outcomes: 178, The best outcome selection method: Greedy algorithm.	$O\left(PK+I+O\right)$

(Continued)

Table 4 (continued)

Phase	Method	Parameters	Time Burden
XAI	DLob	Number of the utilized DLob symbols: 8, The utilized statistical methods: Transition table and information entropy computation, Connectome diagram generation method: Visualizing transition table.	$O(S)$

Notes: The meaning of the symbols used in this table are given as follows. E: the size of the EEG signal, N: time complexity coefficient of the NCA feature selection function, F: length of the features, P: the number of the parameters, K: the time complexity of the kNN, I: time complexity of the IMV method, O: the number of outcomes, S: the number of the selected features. Abbreviations: IMV, iterative majority voting; XAI, explainable artificial intelligence; NCA, neighborhood component analysis; kNN, k-nearest neighbors.

Table 4 lists the settings needed to reproduce the implementation and summarizes the associated computational terms. Under this formulation, the total time complexity of the mBTP-centric XFE model is $O(E + N + F + PK + I + O + S)$, which is consistent with the intended lightweight design.

Five evaluation cases were defined so that the framework could be examined in one multiclass task and four neutral-vs.-emotion binary tasks:

Case 1: All 4895 EEG segments are used in the five-class task (Neutral, Happy, Sad, Angry, and Surprise).

Case 2: Happy detection is formulated as Neutral vs. Happy, containing 1958 EEG segments (978 Neutral and 980 Happy).

Case 3: Sad detection is formulated as Neutral vs. Sad, containing 1956 EEG segments (978 Neutral and 978 Sad).

Case 4: Angry detection is formulated as Neutral vs. Angry, containing 1958 EEG segments (978 Neutral and 980 Angry).

Case 5: Surprise detection is formulated as Neutral vs. Surprise, containing 1957 EEG segments (978 Neutral and 979 Surprise).

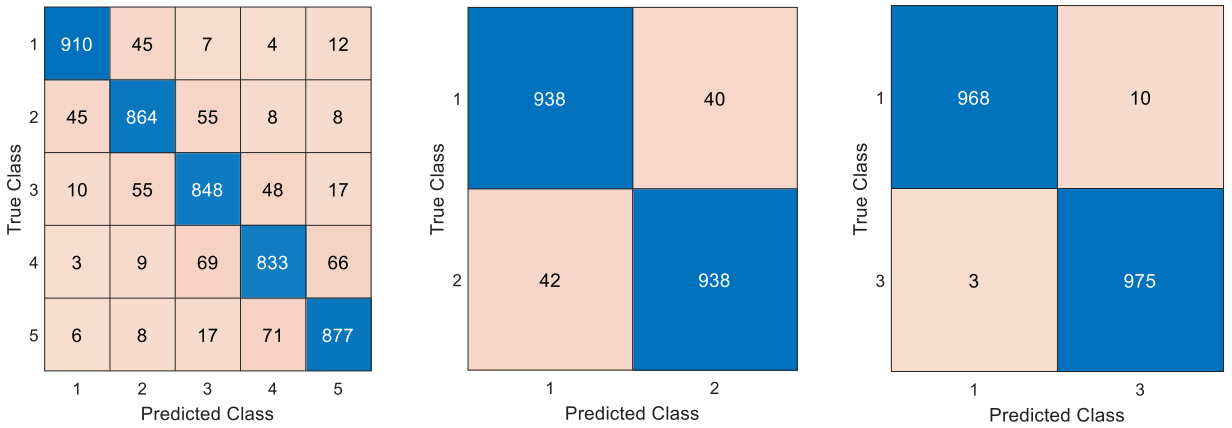
5.1 Classification Results

Classification is the first output of the mBTP-centric XFE pipeline. tkNN was evaluated with two internal validation schemes: segment-level 10-fold CV and record-level LORO CV. Accuracy and geometric mean were calculated from the confusion matrices for the five predefined cases. Fig. 4 presents the 10-fold CV matrices, and Fig. 5 presents the LORO matrices.

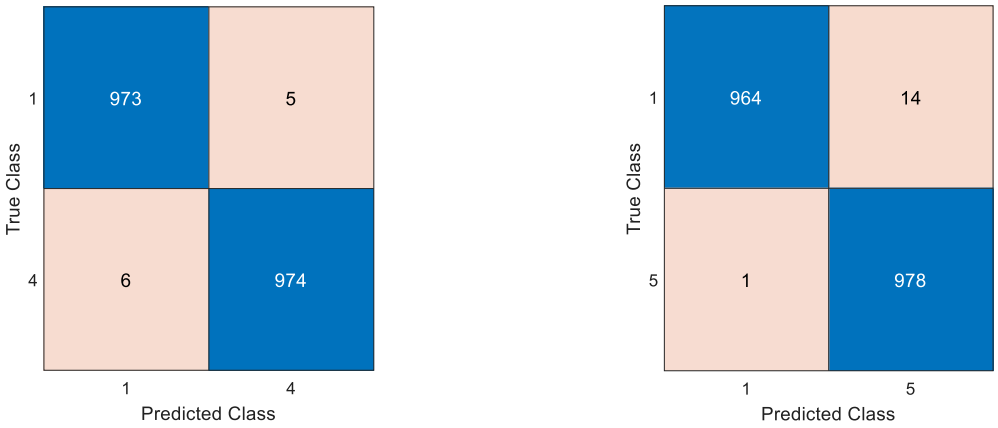
Fig. 5 reports the confusion matrices obtained under record-level LORO CV.

The performance measures derived from these confusion matrices are reported in Table 5.

For the five-class task, segment-level 10-fold CV produced 4332 correct predictions out of 4895 segments, corresponding to 88.50% accuracy (Wilson 95% CI: 87.57–89.36%). Record-level LORO produced 3677 correct predictions, or 75.12% accuracy (Wilson 95% CI: 73.89–76.31%). The 13.38-percentage-point gap is consistent with the greater difficulty of holding out complete records. LORO is nevertheless not equivalent to participant-level LOSO because different records from the same participant may appear in training and test sets.

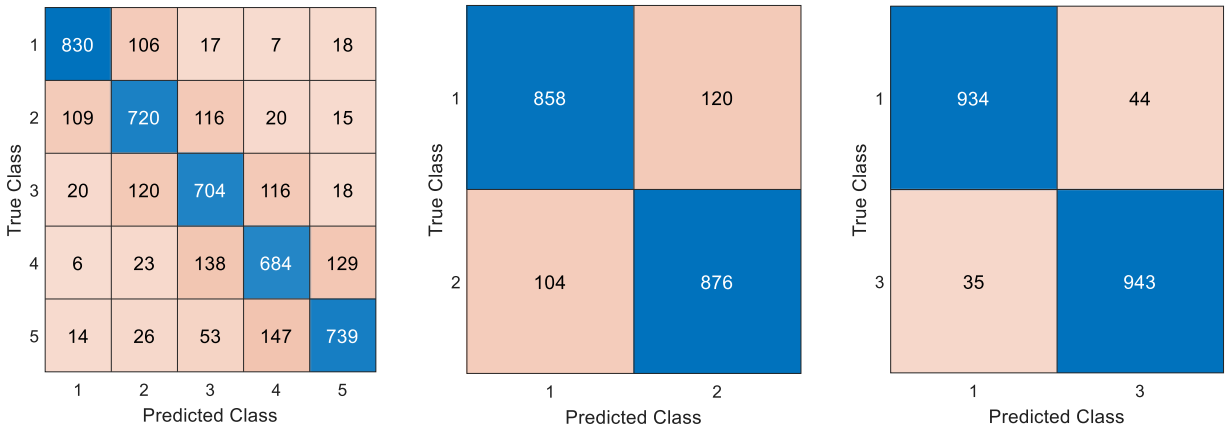


(**a**) Case 1 (**b**) Case 2 (**c**) Case 3



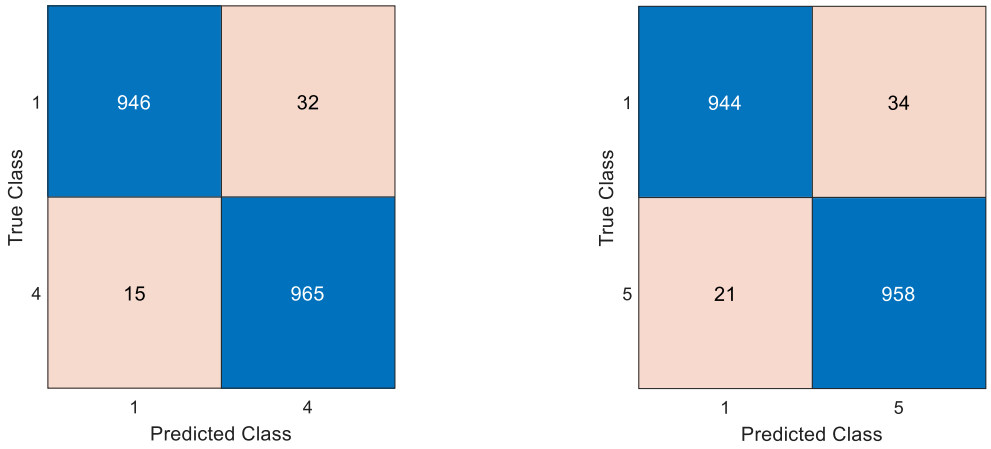
(**d**) Case 4 (**e**) Case 5

Figure 4: The computed confusion matrices deploying the presented mBTP-centric XFE model using 10-fold CV. herein, 1: neutral, 2: happy, 3: sad, 4: angry, 5: surprise.



(**a**) Case 1 (**b**) Case 2 (**c**) Case 3

Figure 5: (Continued)



(**d**) Case 4 (**e**) Case 5

Figure 5: Confusion matrices of the proposed mBTP-centric XFE framework using leave-one-record-out (LORO) cross-validation for (**a**) Five-class emotion recognition, (**b**) Happy detection, (**c**) Sad detection, (**d**) Angry detection, and (**e**) Surprise detection. Class labels are 1: neutral, 2: happy, 3: sad, 4: angry, and 5: surprise.

Table 5: The classification results of the presented mBTP-driven XFE framework.

Case	Validation			
	10-Fold CV		LORO CV	
	Geometric Mean (%)	Accuracy (%)	Geometric Mean (%)	Accuracy (%)
1	88.46	88.50	74.95	75.12
2	95.81	95.81	88.56	88.56
3	99.33	99.34	95.96	95.96
4	99.44	99.44	97.60	97.59
5	99.23	99.23	97.19	97.19

The Wilson intervals quantify uncertainty around the observed segment-level accuracy proportions only. They do not measure variation across independent random seeds. A paired t-test or Wilcoxon signed-rank test between feature extractors would require matched fold- or seed-level outcomes from repeated runs. Because matched fold- or seed-level outcomes were unavailable for the ablation experiments, inferential comparisons were not performed; the ablation results are therefore interpreted descriptively.

Appendix A gives the controlled ablation results under the same five-class segment-level 10-fold protocol. BP + CWNCA + tkNN reached 82.29%, LBP + CWNCA + tkNN 84.11%, mBTP + NCA + tkNN 86.09%, mBTP + CWNCA + single kNN 86.82%, and the complete mBTP + CWNCA + tkNN pipeline 88.50%. Relative to the full model, these settings reduce accuracy by 6.21, 4.39, 2.41, and 1.68 percentage points, respectively. Because only aggregate predictions/counts were available, these differences are reported as descriptive effect sizes rather than seed-level significance tests.

5.2 Explainable Results

The framework also returns an interpretable DLob representation. For each case, the selected mBTP feature identities are mapped to a DLob string. The string is then summarized with a symbol histogram, a transition-based connectome diagram, and Shannon entropy.

The DLob strings shown in Fig. 6 were used to calculate the information-entropy and complexity values reported in Table 6.

Table 6 shows the largest complexity value for Case 3 (88.09%) and the smallest for Case 5 (86.03%).

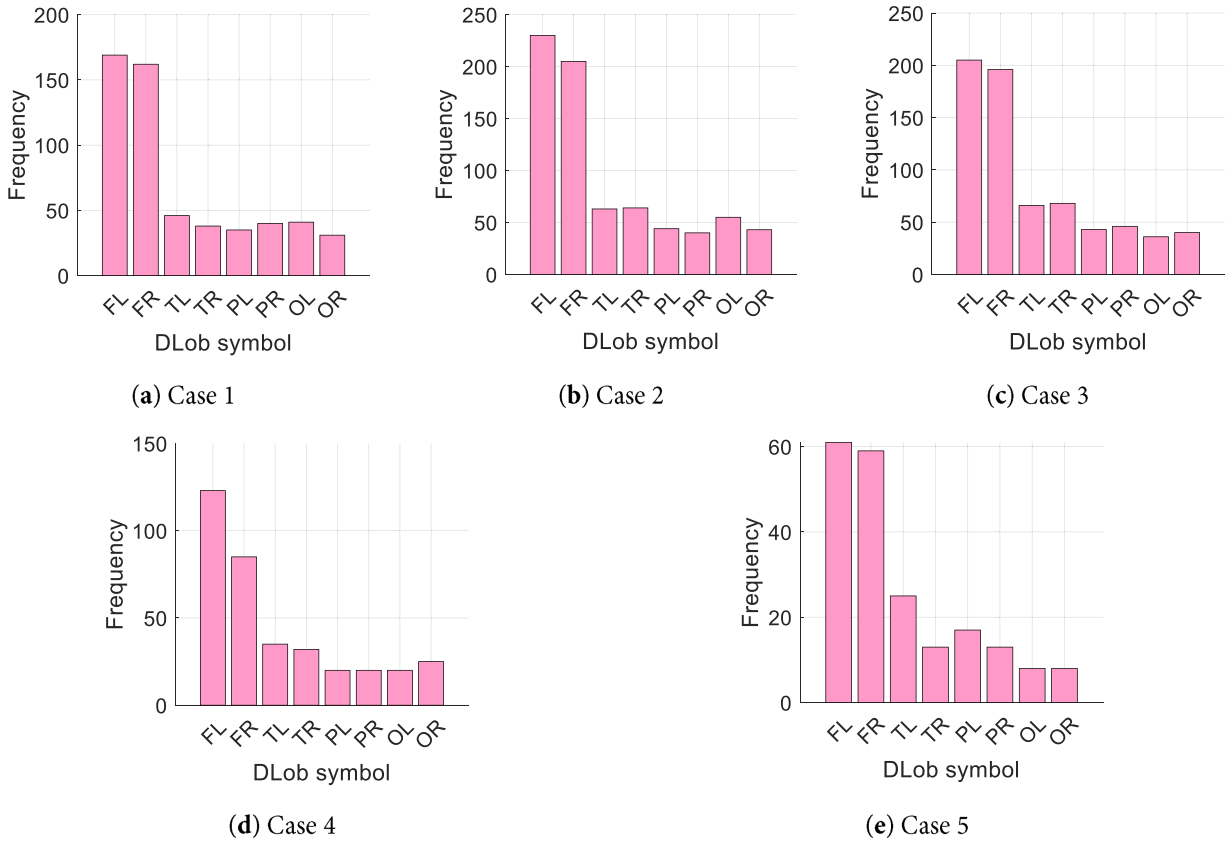
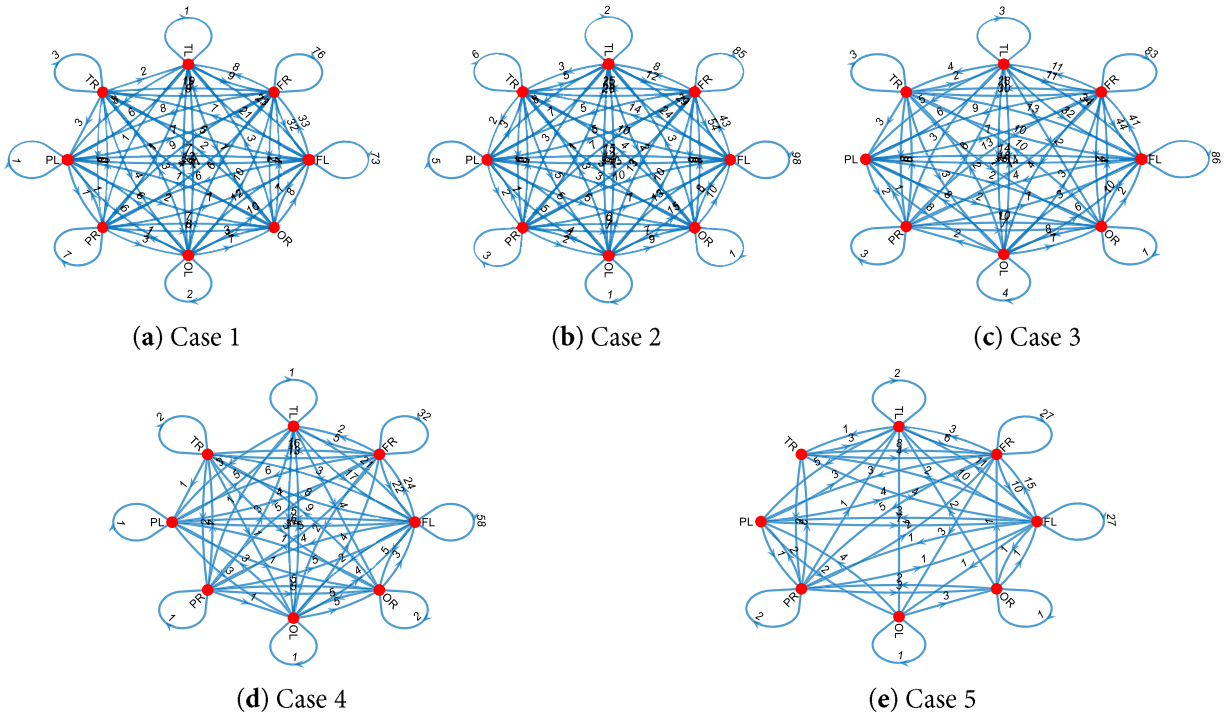


Figure 6: Frequency distributions of the directed lobish (DLob) symbols selected for the five experimental cases: (**a**) Five-class emotion recognition, (**b**) Happy detection, (**c**) Sad detection, (**d**) Angry detection, and (**e**) Surprise detection. The histograms show the relative involvement of the frontal, temporal, parietal, and occipital regions represented by the DLob symbols.

Table 6: The information entropies and complexities of the generated DLob strings.

Case	Information Entropy	Complexity (%)
1	2.6238	87.46
2	2.6256	87.52
3	2.6426	88.09
4	2.6206	87.35
5	2.5810	86.03

Fig. 7 presents the corresponding cortical connectome diagrams.



(**a**) Case 1 (**b**) Case 2 (**c**) Case 3

(**d**) Case 4 (**e**) Case 5

Figure 7: Cortical connectome diagrams generated from DLob symbol transitions for (**a**) Five-class emotion recognition, (**b**) Happy detection, (**c**) Sad detection, (**d**) Angry detection, and (**e**) Surprise detection. Nodes represent cortical regions, and the connections indicate transition frequencies between the corresponding DLob symbols.

The DLob connectomes summarize transitions among the selected channel-level symbols. They are descriptive XAI views of the feature identities and should not be treated as source-localized functional-connectivity measurements. The case-level patterns are interpreted with this limitation in mind.

6 Discussions

Across the five tasks, the mBTP-driven XFE pipeline produced two outputs: a classification result and a symbolic channel-transition summary. The discussion below considers these outputs separately.

6.1 Discussion of Classification Results

In Case 1, the five-class task reached 88.50% with segment-level 10-fold CV and 75.12% with record-level LORO. The four binary tasks were easier, with 10-fold accuracies from 95.81% to 99.44% and LORO accuracies from 88.56% to 97.59%. These differences are task specific and should not be interpreted as evidence of participant-independent generalization.

6.2 Discussions of Interpretable Results

DLob provides the descriptive interpretation branch of the pipeline. For each task, selected feature identities are translated into DLob symbols and counted as channel-level transition patterns. The resulting complexity ratios range from 86.03% to 88.09%. These values reflect the diversity of selected symbolic transitions, not physiological complexity of the underlying emotional state.

Case 3 (sad detection) has the highest DLob complexity ratio at 88.09%, while Case 1 has a ratio of 87.46%. The narrow spread across cases suggests that the selected symbolic representations have broadly similar diversity even when classification accuracy differs.

Frontal DLob symbols occur most often across the five cases, followed by temporal symbols. Because these counts arise from selected sensor-transition identities, they indicate which channel-level features were favored by the model; they are not direct measures of regional brain activation.

The DLob diagrams offer a compact view of the symbol-pair transitions retained by feature selection. Table 7 therefore summarizes, for each case, the most frequent and least frequent transitions together with the number of observed connections. These counts describe the selected feature representation only.

Table 7: Connection analysis for cases.

Case	The Most Connected	The Least Connected	Number of Connections
1	FR-FR: 76 transitions	TL-TR: 0 transitions, PL-TR: 0 transitions, OR-OR: 0 transitions.	61
2	FL-FL: 98 transitions	PR-TL: 1 transition, PR-PL: 1 transition, OL-OL: 1 transition, OR-OR: 1 transition.	64 (Fully connected)
3	FL-FL: 86 transitions	OR-TL: 0 transitions, PL-TR: 0 transitions, PL-PL: 0 transitions, PR-OL: 0 transitions.	60
4	FL-FL: 58 transitions	OR-FR: 0 transitions, TR-TL: 0 transitions, OR-TL: 0 transitions, TL-TR: 0 transitions, PL-TR: 0 transitions, OL-TR: 0 transitions, PR-PL: 0 transitions, PL-PR: 0 transitions, OL-FR: 0 transitions, FR-OR: 0 transitions.	54
		OL-FL: 0 transitions, OL-FR: 0 transitions, OL-TL: 0 transitions, TR-TR: 0 transitions, PL-TR: 0 transitions, OL-TR: 0 transitions, OR-TR: 0 transitions, TR-PL: 0 transitions,	

(Continued)

Table 7 (continued)

Case	The Most Connected	The Least Connected	Number of Connections
5	FL-FL: 27 transitions, FR-FR: 27 transitions	PL-PL: 0 transitions, OR-PL: 0 transitions, TL-PR: 0 transitions, OL-PR: 0 transitions, TR-OL: 0 transitions, PR-OL: 0 transitions, OR-OL: 0 transitions, FR-OR: 0 transitions, TL-OR: 0 transitions, TR-OR: 0 transitions, PL-OR: 0 transitions.	45

Table 7 shows that all 64 possible symbol-pair connections are represented in Case 2, whereas Case 5 contains 45 observed connections. This contrast reflects the density of the selected DLob transition set and does not imply that one emotional state requires more physiological connectivity than another.

6.3 Comparative Results

Table 8 places the present results beside representative EEG emotion-recognition studies to provide context rather than a direct ranking.

Table 8: The comparative results.

Study	Dataset	Method	XAI	Validation Scheme	The Results (%)
Fu et al. [13]	SEED (15 subjects)	Dynamic graph attention network	No	Leave-one-subject-out (LOSO)	Acc: 85.86
Bagherzadeh et al. [14]	1. DEAP (32 subjects) 2. MAHNOB-HCI (24 subjects)	Direct directed transfer function, convolutional neural networks (CNN)	No	LOSO	1. Acc:98.76 Pre: 98.57 Sen: 98.79 F1: 98.66 2. Acc: 98.86 Pre: 98.83 Sen: 98.79 F1: 98.88
Cai et al. [15]	1. SEED (15 subjects), 2. SEED IV (15 subjects)	EEG Swin Transformer	No	LOSO	Subject-dependent 1. Acc:94.83 2. Acc:79.45 Subject-independent 1. Acc:80.07 2. Acc:66.72
Han et al. [16]	DEAP (32 subjects—153,600 samples)	Multi-scale emotion recognition method	No	10-fold CV	Subject-dependent 1. Acc:91.31 Subject-independent 1. Acc:86.66
Bardak et al. [17]	1. Collected data (2 subjects) 2. DEAP (32 subjects)	Adaptive neuro-fuzzy	No	5-fold CV	1. Acc:95.97 2. Acc:73.49

(Continued)

Table 8 (continued)

Study	Dataset	Method	XAI	Validation Scheme	The Results (%)
Yu et al. [18]	1. SEED (15 subjects), 2. SEED IV (15 subjects)	Multi-source domain adaptation	No	a. Cross subject b. Cross session	1a. Acc:90.96 1b. Acc:91.94 2a. Acc:76.01 2b. Acc:78.78
Shi and Liu [19]	1. DEAP (32 subjects) 2. DREAMER (23 subjects) 3. SEED (15 subjects)	Interactive multi-agent convolutional broad learning system	No	5-fold CV	1. Acc:82.86 2. Acc:98.49 3. Acc:85.09
Dai et al. [20]	1. DEAP (32 subjects) 2. SEED (15 subjects)	1D CNN	No	5-fold CV	1. Acc:95.23% (valence), 96.31% (arousal) 2. Acc:95.16
Xiao et al. [21]	1. SEED (15 subjects), 2. SEED IV (15 subjects)	Multi-source dynamic contrastive domain adaptation method	No	Leave-one-out CV	1.Acc: 95.82 2.Acc: 82.25
Cruz-Vazquez et al. [22]	Collected data (40 subjects)	Advanced Transformations, Fourier Neural Networks and quantum rotations	No	Unspecified	Acc: 95.00
Zhang et al. [23]	1. DEAP (32 subjects) 2. SEED (15 subjects)	Multiple attention mechanisms, long short term memory	No	5-fold CV	1. Acc: 92.41 for valence 92.71 for arousal 2. Acc: 93.93
Sun et al. [24]	HR-EEG4EMO	Dynamic brain function network	No	1. 9-fold CV 2. 5-fold CV	1. Acc: 83.50 2. Acc: 88.93
Wang et al. [25]	1. DEAP (32 subjects) 2. DREAMER (23 subjects) 3. SEED (15 subjects)	Joint-dimension-aware transformer	No	10-fold CV	1. Acc: 98.51 F1: 97.52 2. Acc: 98.01 F1: 96.92 3. Acc: 97.30 F1: 97.14
Tan et al. [26]	1. SEED (15 subjects), 2. SEED IV (15 subjects)	Semi-supervised and domain adversarial learning	No	Leave-one-out CV	1. Acc: 86.39 2. Acc: 77.80
Gao et al. [27]	DEAP (32 subjects)	Robust principal component analysis	No	10-fold CV	Acc: 93.04 for valence 93.13 for arousal
Chen et al. [28]	1. DEAP (32 subjects) 2. SEED (15 subjects)	3D feature fusion network	No	10-fold CV	1. Acc: 83.54 for valence 84.93 for arousal 2. Acc: 96.64
Chaudary et al. [29]	SEED (15 subjects)	Gradient class activation map, CNN	Yes	5-fold CV	Acc: 99.31
Hu et al. [30]	1. FACED (123 subjects) 2. THU-EP (80 subjects) 3. SEED (15 subjects)	Contrastive learning	No	10-fold CV	1. FACED: 72.50% (binary) 2. THU-EP: 76.20% (nine-class) 3. SEED: 88.30% (three-class)
Ju et al. [31]	1. SEED (15 subjects), 2. SEED IV (15 subjects)	Domain adversarial learning	No	Leave-one-out CV	1. Acc: 95.74 2. Acc:86.75

(Continued)

Table 8 (continued)

Study	Dataset	Method	XAI	Validation Scheme	The Results (%)
Cao et al. [32]	1. TJU-EmoEEG (10 subjects) 2. SEED (15 subjects)	Dynamic spatial-spectral-temporal network, graph CNN	No	Subject-dependent	1. Acc: 86.20 F1: 85.50 2. Acc: 95.20 F1: 94.80
Xu et al. [33]	1. DEAP (32 subjects) 2. DREAMER (23 subjects) 3. PhyMER (30 subjects)	Deep-wise separable convolution, retention transformer	No	10-fold CV	1. Acc: 77.11 F1: 75.39 for valence Acc: 76.71 F1: 75.15 for arousal 2. Acc: 82.78 F1: 83.59 for valence Acc: 80.79 F1: 81.63 for arousal 3. Acc: 86.41 F1: 83.47 for valence Acc: 82.13 F1: 80.18 for arousal
Li et al. [34]	DEAP (32 subjects)	Deep multi-view CNN	No	5-fold CV	Acc: 97.55 for valence 97.61 for arousal
Chang et al. [35]	1. SEED (15 subjects) 2. MPED (30 subjects) 3. FACED (123 subjects)	Multi-scale hyperbolic contrastive learning	No	LOSO	1. Acc: 89.30 2. Acc: 38.80 3. Acc: 77.00
Chen et al. [36]	1. DEAP (32 subjects) 2. DREAMER (23 subjects)	3D CNN-CapsNet	No	5-fold CV	1. Acc: 97.40 for valance 97.20 for arousal 97.60 for dominance 2. Acc: 95.80 for valance 96.10 for arousal 96.30 for dominance
Yan et al. [37]	1. DEAP (32 subjects) 2. SEED (15 subjects)	Spatio-temporal Graph Bert network	No	1. 59:41 2. 70:30	1. Acc:80.32% (arousal), 81.64% (valence) 2. Acc: 89.39
Khan et al. [51]	1.DEAP (32 subjects) 2. SEED	CWT-based time–frequency feature extraction, spatio-temporal representation, 3D CNN with multiscale kernels	Yes	10-fold CV	1. Arousal Acc: 96.13; Valence Acc: 96.19. 2. Arousal Acc: 97.42; Valence Acc: 97.50
Khan et al. [52]	1. SEED 2. DEAP	DAFNet: dual-path attention fusion using DE-based 2D CNN and SCS-based graph attention/global covariance modeling	No	Train/test evaluation with external validation	1. Acc: 97.73. 2. Acc: 97.89
Our study	Collected: 4895 segments; 49 participants; 245 records	mBTP	Yes	Segment 10-fold CV; record LORO (not LOSO)	Case 1 only: 10-fold Acc 88.50, GM 88.46; LORO Acc 75.12, GM 74.95. Cases 2–5: Table 5.

Note: Abbreviations: Acc, accuracy; Pre, precision; Sen, sensitivity; F1, F1 score; CV, cross-validation; LOSO, leave-one-subject-out; CNN, convolutional neural network; XAI, explainable artificial intelligence.

Table 8 is intended as a descriptive comparison. The listed studies differ in dataset, number of classes, preprocessing, channel configuration, and validation unit, so their accuracy values are not directly

comparable. For the present method, the table reports only the five-class Case 1 result and labels 75.12% explicitly as record-level LORO rather than LOSO.

6.4 Research Significance

Findings:

- A five-class EEG emotion dataset based on sentence elicitation was collected for this work. Because many established EER resources use audiovisual stimuli, this protocol offers a complementary text-based setting.
- mBTP extends the BP idea from scalar comparisons to multichannel vector differences, followed by channel ordering and transition-table construction.
- The complete XFE pipeline links mBTP, CWNCA, tkNN, and DLob so that classification accuracy and channel-level interpretability can be examined within the same workflow.
- All five tasks achieved more than 75% accuracy under both internal validation schemes. These figures describe segment- and record-level performance only; participant-independent generalization is not claimed.
- For Case 1, FR-FR is the most frequent selected transition. The 61 observed symbol-pair connections indicate a relatively dense channel-level representation, but they do not constitute evidence of localized cortical activation.
- For happy detection (Case 2), FL-FL is the most frequent selected transition. All 64 DLob symbol-pair connections are represented, giving this task the densest selected transition set. This is a descriptive feature-selection result rather than evidence of neural synchronization or a causal mechanism.
- For sad detection (Case 3), FL-FL again has the highest count. The absent PL-PL and PL-TR edges mean that these symbol pairs were not represented among the selected transitions; they do not show that parietal sensory integration is absent during sadness.
- For angry detection (Case 4), FL-FL remains the most frequent selected transition, although its count is lower than in Cases 2 and 3. Several temporal and occipital pairs are missing from the selected set, which describes the model representation rather than emotion physiology.
- For surprise detection (Case 5), FL-FL and FR-FR share the highest count. The graph contains 45 observed symbol-pair connections, fewer than the other cases, indicating a more restricted selected-transition representation without implying a source-localized mechanism.

Advantages:

- The study provides a lightweight feature-engineering pipeline with strong internal classification results.
- DLob produces a channel-level symbolic summary alongside the classifier output. This built-in interpretation is useful for tracing selected feature relationships, while remaining distinct from source-localized connectivity analysis.
- The auxiliary route ablation identifies a practical efficiency point: four mBTP routes require 784 features, exactly half of the full 1568-dimensional representation. On the separate artifact dataset, this compact setting is only 0.16 percentage points below the eight-route result, which motivates further testing of compact mBTP on the emotion dataset.
- The method is computationally modest and interpretable. No claim of direct superiority over deep networks is made because the comparison studies use different datasets and validation protocols.

Limitations:

- The cohort includes 49 Turkish participants aged 19–26 years, so demographic and language generalization is still limited.

- The full mBTP-CWNCA-tkNN pipeline has not yet been evaluated on a matched public EEG emotion benchmark. Appendix B uses a separate artifact dataset only as a cross-task representation check and does not establish public-benchmark emotion performance.
- The reported 10-fold CV is segment based, whereas LORO holds out complete records. Neither split guarantees participant-disjoint training and testing. Participant-level identifiers were not available for the current analytical dataset; consequently, participant-disjoint LOSO evaluation could not be performed.
- The available ablation results consist of aggregate prediction outcomes; therefore, repeated-seed variability and paired inferential statistics are not reported
- Channel-wise standard-deviation and frequency-band summaries are not reported because the raw channel-level waveforms were not included in the available analysis file. Rather than estimate these values, the descriptive signal analysis is reserved for reconstruction from the original recordings.
- DLob operates at the channel-symbol level on a 14-channel consumer EEG montage. Its connectome diagrams are descriptive maps of selected transitions, not source-localized functional-connectivity estimates.

Future directions:

- Validate the pipeline in larger, more diverse cohorts, including non-Turkish language settings and independent acquisition sites.
- Repeat the five-class BP, LBP, and mBTP experiments with 10 predefined seeds and identical folds for each seed; report mean +/− SD and two-sided Wilcoxon signed-rank tests for mBTP vs. BP and mBTP vs. LBP, followed by Holm correction.
- Reconstruct participant grouping from the raw recordings and run 49-fold participant-level LOSO, reporting participant-level and segment-level results separately.
- Apply the full preprocessing-mBTP-CWNCA-tkNN pipeline to established public EEG emotion datasets such as DEAP, SEED, or DREAMER with subject-wise validation, and report dataset-specific comparisons under matched protocols.
- Reconstruct the raw channel-level recordings for descriptive signal analysis, including channel-wise amplitude variability and delta, theta, alpha, beta, and gamma band-power summaries. Broader baseline testing, device robustness, and real-time validation should follow these primary validation steps.

Potential applications:

- After prospective validation, the pipeline may support research on real-time EEG-based emotion monitoring.
- Validated affect estimates may also be useful in adaptive human-computer interfaces and personalized smart-device interaction.
- In gaming research, validated affect estimates could be used to adapt feedback or interaction dynamics.
- Educational studies could test whether EEG-derived affect estimates are useful for adaptive content delivery.
- The same framework may also help quantify affective responses to sentence-based stimuli in controlled research settings.

7 Conclusions

This study introduced multichannel Binary Transition Pattern (mBTP) and combined it with CWNCA, tkNN, and DLob in a lightweight XFE pipeline. On the 4895-segment five-class task, the full configuration achieved 88.50% under segment-level 10-fold CV and 75.12% under record-level LORO. Controlled ablation reduced accuracy to 82.29% with BP, 84.11% with LBP, 86.09% when CWNCA was replaced by NCA,

and 86.82% when tkNN was replaced by a single kNN. These findings support the contribution of the multichannel representation, feature selection, and ensemble classifier within the current internal validation setting. The auxiliary artifact analysis further showed that a four-route compact mBTP variant used half as many features as the eight-route representation while differing by only 0.16 percentage points on that separate task. Participant-disjoint LOSO, repeated-seed inference, raw-signal descriptive analysis, and matched public emotion-benchmark evaluation are still required before broader generalization claims can be made.

Acknowledgement: We thank the participants and Firat University for institutional support during data collection and transcription.

Funding Statement: This study was supported by the TF.25.66 project fund of the Scientific Research Projects Coordination Unit of Firat University.

Author Contributions: Conceptualization, Abdullahi Abba Abdullahi, Suat Tas, Dahiru Tanko, Gullu Boztas, Burak Tasci, İrem Taşcı, Sengul Dogan, Turker Tuncer; methodology, Abdullahi Abba Abdullahi, Suat Tas, Dahiru Tanko, Gullu Boztas, Burak Tasci, İrem Taşcı, Sengul Dogan, Turker Tuncer; software, Sengul Dogan, Turker Tuncer; validation, Abdullahi Abba Abdullahi, Suat Tas, Dahiru Tanko, Gullu Boztas, Sengul Dogan, Turker Tuncer; formal analysis, Abdullahi Abba Abdullahi, Suat Tas, Dahiru Tanko, Gullu Boztas, Sengul Dogan, Turker Tuncer; investigation, Abdullahi Abba Abdullahi, Suat Tas, Dahiru Tanko; resources, Abdullahi Abba Abdullahi, Suat Tas, Dahiru Tanko, Gullu Boztas, Sengul Dogan, Turker Tuncer; data curation, Abdullahi Abba Abdullahi, Suat Tas, Dahiru Tanko; writing—original draft preparation, Abdullahi Abba Abdullahi, Suat Tas, Dahiru Tanko, Gullu Boztas, Burak Tasci, İrem Taşcı, Sengul Dogan, Turker Tuncer; writing—review and editing, Abdullahi Abba Abdullahi, Suat Tas, Dahiru Tanko, Gullu Boztas, Burak Tasci, İrem Taşcı, Sengul Dogan, Turker Tuncer; visualization, Abdullahi Abba Abdullahi, Suat Tas, Dahiru Tanko; supervision, Turker Tuncer; project administration, Turker Tuncer. All authors reviewed and approved the final version of the manuscript.

Availability of Data and Materials: Participant-level raw EEG data from the emotion-recognition dataset can be requested from the corresponding author, subject to ethics and institutional approval. The separate eight-class EEG artifact dataset used for the auxiliary analysis in Appendix B, previously described in Reference [48], can also be requested from the corresponding author, subject to the applicable ethical and institutional restrictions. To support reproducibility, the analysis code and, where permitted, derived feature matrices and prediction outputs can also be provided on reasonable request.

Ethics Approval: The Non-Invasive Ethics Committee of Firat University approved the study on 04 November 2021 (2021/11-34). The protocol followed the principles of the Declaration of Helsinki. Written informed consent was obtained from every participant included in the study.

Conflicts of Interest: The authors declare no conflicts of interest.

Appendix A Controlled Ablation Analysis

All configurations in Table A1 use the same 4895-segment five-class task and the same segment-level 10-fold validation procedure. Only the component named in each row is changed, allowing the contributions of the feature extractor, selector, and classifier to be examined under a fixed protocol.

The complete pipeline gives the highest accuracy. Compared with that result, BP is lower by 6.21 percentage points, LBP by 4.39 points, NCA by 2.41 points, and a single kNN by 1.68 points. These values are descriptive differences based on aggregate held-out predictions. Because matched repeated-seed outputs were not retained, the table does not support a paired significance claim.

Table A1: Controlled ablation results for the five-class emotion task.

Configuration	Accuracy (%)	Wilson 95% CI	Role
BP + CWNCA + tkNN	82.29	81.19–83.33	Feature-extractor baseline
LBP + CWNCA + tkNN	84.11	83.06–85.10	Feature-extractor baseline
mBTP + NCA + tkNN	86.09	85.09–87.03	CWNCA ablation
mBTP + CWNCA + single kNN	86.82	85.85–87.74	tkNN ablation
mBTP + CWNCA + tkNN	88.50	87.57–89.36	Full model

Appendix B Auxiliary mBTP Route-Efficiency Ablation on an EEG Artifact Dataset

A separate eight-class EEG artifact dataset previously used with Directed Lobish/TTPat (48) was used for a cross-task representation check. It contains 2498 five-second segments from 14 channels sampled at 128 Hz. For this appendix, only cumulative mBTP routes were evaluated with fold-local min-max scaling and a fixed 1-NN cityblock classifier under stratified 10-fold CV. CWNCA and tkNN voting were intentionally excluded so that the route representation itself could be examined. The cumulative mBTP route-ablation results are summarized in Table A2.

Table A2: Representation-only cumulative mBTP route ablation on the separate EEG artifact dataset.

Routes	Features	Accuracy (%)	10-Fold Mean ± SD (%)	Wilson 95% CI
1	196	73.10	73.10 ± 2.13	71.33–74.80
2	392	77.86	77.86 ± 2.44	76.19–79.45
3	588	81.67	81.67 ± 2.30	80.10–83.13
4	784	83.91	83.91 ± 2.12	82.41–85.30
5	980	83.75	83.75 ± 2.65	82.25–85.14
6	1176	83.47	83.47 ± 2.32	81.96–84.87
7	1372	83.95	83.95 ± 2.35	82.46–85.33
8	1568	84.07	84.07 ± 2.64	82.58–85.45

Accuracy increases from 73.10% with one route to 83.91% with four routes and 84.07% with all eight. The four-route setting uses 784 features, exactly half of the 1568-feature representation, while its accuracy is only 0.16 percentage points lower on this separate artifact task. Routes five through eight therefore add little net gain here and the changes are not monotonic.

For efficiency-focused follow-up work, the four-route setting is referred to as compact mBTP. The primary emotion experiments still use all eight routes because those experiments were completed with the full representation. The compact variant should therefore be treated as an auxiliary finding until it is evaluated on the emotion dataset under the same protocol.

References

1. Dev P, Pathak A. Characterization of biomedical signals in neurological disorders. In: Cognitive predictive maintenance tools for brain diseases. Boca Raton, FL, USA: Chapman and Hall/CRC; 2023. p. 56–72. doi:10.1201/9781003245346-4.
2. Samal P, Hashmi MF. Role of machine learning and deep learning techniques in EEG-based BCI emotion recognition system: a review. Artif Intell Rev. 2024;57(3):50. doi:10.1007/s10462-023-10690-2.

3. Kumar S, Sharma A. Advances in non-invasive EEG-based brain-computer interfaces: signal acquisition, processing, emerging approaches, and applications. In: Signal processing strategies. Amsterdam, The Netherland: Elsevier; 2025. p. 281–310. doi:10.1016/b978-0-323-95437-2.00014-8.
4. Yu X, Li W, Yang B, Li X, Chen J, Fu G. Periodic distribution entropy: unveiling the complexity of physiological time series through multidimensional dynamics. Inf Fusion. 2024;108:102391. doi:10.1016/j.inffus.2024.102391.
5. Fang L, Li Y, Shao M, Yu A, Felemban BF, Aly AA, et al. Enhancing medical signal processing and diagnosis with AI-generated content techniques. IEEE J Biomed Health Inform. 2025;29(12):9245–58. doi:10.1109/jbhi.2024.3429560.
6. Theng D, Bhoyar KK. Feature selection techniques for machine learning: a survey of more than two decades of research. Knowl Inf Syst. 2024;66(3):1575–637. doi:10.1007/s10115-023-02010-5.
7. Hosain MT, Jim JR, Mridha MF, Kabir MM. Explainable AI approaches in deep learning: advancements, applications and challenges. Comput Electr Eng. 2024;117:109246. doi:10.1016/j.compeleceng.2024.109246.
8. Erat K, Şahin EB, Doğan F, Merdanoğlu N, Akcakaya A, Durdu PO. Emotion recognition with EEG-based brain-computer interfaces: a systematic literature review. Multimed Tools Appl. 2024;83(33):79647–94. doi:10.1007/s11042-024-18259-z.
9. Fan C, Wang J, Huang W, Yang X, Pei G, Li T, et al. Light-weight residual convolution-based capsule network for EEG emotion recognition. Adv Eng Inform. 2024;61:102522. doi:10.1016/j.aei.2024.102522.
10. Xu X, Wei F, Jia T, Zhuo L, Zhang H, Li X, et al. Embedded EEG feature selection for multi-dimension emotion recognition via local and global label relevance. IEEE Trans Neural Syst Rehabil Eng. 2024;32:514–26. doi:10.1109/tnsre.2024.3355488.
11. Cho J, Hwang H. Spatio-temporal representation of an electoencephalogram for emotion recognition using a three-dimensional convolutional neural network. Sensors. 2020;20(12):3491. doi:10.3390/s20123491.
12. Liu H, Zhang S, Shi J, Liu H, Zhang Y, Wu W, et al. EEG emotion recognition via a lightweight 1DCNN-BiLSTM model in resource-limited environments. IEEE Sens J. 2025;25(3):5723–30. doi:10.1109/jsen.2024.3514094.
13. Fu R, Cai M, Wang S, Wang Y, Jia C. Exploring non-Euclidean relationships in EEG emotion recognition: a dynamic graph attention network. Biomed Signal Process Control. 2024;94:106276. doi:10.1016/j.bspc.2024.106276.
14. Bagherzadeh S, Shalbaf A, Shoeibi A, Jafari M, Tan RS, Acharya UR. Developing an EEG-based emotion recognition using ensemble deep learning methods and fusion of brain effective connectivity maps. IEEE Access. 2024;12:50949–65. doi:10.1109/ACCESS.2024.3384303.
15. Cai M, Chen J, Hua C, Wen G, Fu R. EEG emotion recognition using EEG-SWTNS neural network through EEG spectral image. Inf Sci. 2024;680:121198. doi:10.1016/j.ins.2024.121198.
16. Han L, Zhang X, Yin J. EEG emotion recognition based on the TimesNet fusion model. Appl Soft Comput. 2024;159:111635. doi:10.1016/j.asoc.2024.111635.
17. Bardak FK, Seyman MN, Temurtaş F. Adaptive neuro-fuzzy based hybrid classification model for emotion recognition from EEG signals. Neural Comput Appl. 2024;36(16):9189–202. doi:10.1007/s00521-024-09573-6.
18. Yu P, He X, Li H, Dou H, Tan Y, Wu H, et al. FMLAN: a novel framework for cross-subject and cross-session EEG emotion recognition. Biomed Signal Process Control. 2025;100:106912. doi:10.1016/j.bspc.2024.106912.
19. Shi S, Liu W. Interactive multi-agent convolutional broad learning system for EEG emotion recognition. Expert Syst Appl. 2025;260:125420. doi:10.1016/j.eswa.2024.125420.
20. Dai S, Li M, Wu X, Ju X, Li X, Yang J, et al. Contrastive learning of EEG representation of brain area for emotion recognition. IEEE Trans Instrum Meas. 2025;74:1–13. doi:10.1109/tim.2025.3533618.
21. Xiao Y, Zhang Y, Peng X, Han S, Zheng X, Fang D, et al. Multi-source EEG emotion recognition via dynamic contrastive domain adaptation. Biomed Signal Process Control. 2025;102:107337. doi:10.1016/j.bspc.2024.107337.
22. Cruz-Vazquez JA, Montiel-Pérez JY, Romero-Herrera R, Rubio-Espino E. Emotion recognition from EEG signals using advanced transformations and deep learning. Mathematics. 2025;13(2):254. doi:10.3390/math13020254.
23. Zhang Y, Qu J, Zhang Q, Cheng C. EEG-based emotion recognition based on 4D feature representations and multiple attention mechanisms. Biomed Signal Process Control. 2025;103:107432. doi:10.1016/j.bspc.2024.107432.
24. Sun H, Wang H, Wang R, Gao Y. Emotion recognition based on EEG source signals and dynamic brain function network. J Neurosci Meth. 2025;415:110358. doi:10.1016/j.jneumeth.2024.110358.

25. Wang Z, Zhou Z, Shen H, Men C, Sun Q, Huang K. JDAT: joint-dimension-aware transformer with strong flexibility for EEG emotion recognition. In: Proceedings of the Third International Conference on Electrical, Electronics, and Information Engineering (EEIE 2024); 2024 Nov 14–16; Wuhan, China. p. 42–52.
26. Tan W, Zhang H, Wang Y, Wen W, Chen L, Li H, et al. SEDA-EEG: a semi-supervised emotion recognition network with domain adaptation for cross-subject EEG analysis. Neurocomputing. 2025;622:129315. doi:10.1016/j.neucom.2024.129315.
27. Gao Y, Xue Y, Gao J. Emotion recognition from multichannel EEG signals based on low-rank subspace self-representation features. Biomed Signal Process Control. 2025;99:106877. doi:10.1016/j.bspc.2024.106877.
28. Chen K, Chai S, Cai M, Liu Q, Ai Q, Zhou C, et al. A novel 3D feature fusion network for EEG emotion recognition. Biomed Signal Process Control. 2025;102:107347. doi:10.1016/j.bspc.2024.107347.
29. Chaudary E, Ahmad Khan S, Mumtaz W. EEG-CNN-Souping: interpretable emotion recognition from EEG signals using EEG-CNN-souping model and explainable AI. Comput Electr Eng. 2025;123:110189. doi:10.1016/j.compeleceng.2025.110189.
30. Hu M, Xu D, He K, Zhao K, Zhang H. Cross-subject emotion recognition with contrastive learning based on EEG signal correlations. Biomed Signal Process Control. 2025;104:107511. doi:10.1016/j.bspc.2025.107511.
31. Ju X, Wu X, Dai S, Li M, Hu D. Domain adversarial learning with multiple adversarial tasks for EEG emotion recognition. Expert Syst Appl. 2025;266:126028. doi:10.1016/j.eswa.2024.126028.
32. Cao L, Zhao W, Sun B. Emotion recognition using multi-scale EEG features through graph convolutional attention network. Neural Netw. 2025;184:107060. doi:10.1016/j.neunet.2024.107060.
33. Xu Z, Chen N, Li G, Li J, Zhu H, Zhu Z. The mitigation of heterogeneity in temporal scale among different cortical regions for EEG emotion recognition. Knowl Based Syst. 2025;309:112826. doi:10.1016/j.knosys.2024.112826.
34. Li Q, Jin D, Huang J, Zhong Q, Xu L, Lin J, et al. DEMA: deep EEG-first multi-physiological affect model for emotion recognition. Biomed Signal Process Control. 2025;99:106812. doi:10.1016/j.bspc.2024.106812.
35. Chang J, Zhang Z, Qian Y, Lin P. Multi-scale hyperbolic contrastive learning for cross-subject EEG emotion recognition. IEEE Trans Affect Comput. 2025;16(3):1716–31. doi:10.1109/TAFFC.2025.3535542.
36. Chen K, Ruan W, Liu Q, Ai Q, Ma L. A novel deep learning model combining 3DCNN-CapsNet and hierarchical attention mechanism for EEG emotion recognition. Neural Netw. 2025;186:107267. doi:10.1016/j.neunet.2025.107267.
37. Yan J, Du C, Li N, Zhou X, Liu Y, Wei J, et al. Spatio-temporal graph bert network for EEG emotion recognition. Biomed Signal Process Control. 2025;104:107576. doi:10.1016/j.bspc.2025.107576.
38. Hu S, Li M, Liu Y, Jiang W, Geng B, Zhong W, et al. Audio-visual perceptual quality measurement via multi-perspective spatio-temporal EEG analysis. Pattern Recognit. 2026;176:113156. doi:10.1016/j.patcog.2026.113156.
39. Jiang W, Zhang Y, Han H, Liu X, Gwak J, Gu W, et al. Fuzzy ensemble-based federated learning for EEG-based emotion recognition in Internet of Medical Things. J Ind Inf Integr. 2025;44:100789. doi:10.1016/j.jii.2025.100789.
40. Lian Y, Zhu M, Sun Z, Liu J, Hou Y. Emotion recognition based on EEG signals and face images. Biomed Signal Process Control. 2025;103:107462. doi:10.1016/j.bspc.2024.107462.
41. Yan F, Guo Z, Iliyasu AM, Hirota K. Multi-branch convolutional neural network with cross-attention mechanism for emotion recognition. Sci Rep. 2025;15:3976. doi:10.1038/s41598-025-88248-1.
42. Liu X, Chen T, Zhou J, Wang H, Liu G, Fu X. Human emotion and StO_2: dataset, pattern, and recognition of basic emotions. Pattern Recognit. 2025;161:111249. doi:10.1016/j.patcog.2024.111249.
43. Pillalamarri R, Shanmugam U. A review on EEG-based multimodal learning for emotion recognition. Artif Intell Rev. 2025;58(5):131. doi:10.1007/s10462-025-11126-9.
44. Erdem Güler S, Patlar Akbulut F. Multimodal emotion recognition: emotion classification through the integration of EEG and facial expressions. IEEE Access. 2025;13:24587–603. doi:10.1109/ACCESS.2025.3538642.
45. Miao M, Liang J, Sheng Z, Liu W, Xu B, Hu W. ST-SHAP: a hierarchical and explainable attention network for emotional EEG representation learning and decoding. J Neurosci Meth. 2025;414:110317. doi:10.1016/j.jneumeth.2024.110317.
46. Fiorini L, Bossi F, Di Gruttola F. EEG-based emotional valence and emotion regulation classification: a data-centric and explainable approach. Sci Rep. 2024;14:24046. doi:10.1038/s41598-024-75263-x.

47. Tuncer T, Dogan S, Baygin M, Tasci I, Mungen B, Tasci B, et al. Directed Lobish-based explainable feature engineering model with TTPat and CWINCA for EEG artifact classification. Knowl Based Syst. 2024;305:112555. doi:10.1016/j.knosys.2024.112555.
48. Goldberger J, Hinton GE, Roweis S, Salakhutdinov RR. Neighbourhood components analysis. In: Advances in neural information processing systems. Red Hook, NY, USA: Curran Associates, Inc.; 2004. p. 513–20.
49. Maillo J, Ramírez S, Triguero I, Herrera F. kNN-IS: an iterative spark-based design of the k-nearest neighbors classifier for big data. Knowl Based Syst. 2017;117:3–15. doi:10.1016/j.knosys.2016.06.012.
50. Dogan A, Akay M, Barua PD, Baygin M, Dogan S, Tuncer T, et al. PrimePatNet87: prime pattern and tunable q-factor wavelet transform techniques for automated accurate EEG emotion recognition. Comput Biol Med. 2021;138:104867. doi:10.1016/j.compbiomed.2021.104867.
51. Khan MR, Tania AA, Ahmad M. A comparative study of time–frequency features based spatio-temporal analysis with varying multiscale kernels for emotion recognition from EEG. Biomed Signal Process Control. 2025;107:107826. doi:10.1016/j.bspc.2025.107826.
52. Khan MR, Tania AA, Bushra TA, Pritha J, Ahmad M. DAFNet: a dual-path attention fusion network for EEG emotion recognition via CNN and graph-based global modeling. Array. 2025;28:100561. doi:10.1016/j.array.2025.100561.